Chapter 2
Experimental Insights into Process–Property Relationships in Binder Jet 3D Printing of Inconel 625

Mohamed A. Abbas, M Faisal Riyad, Sun Woong Kim, Nathan Fonseca, Shams Torabnia, Pu Han, and Keng Hsu

Abstract Conventional manufacturing of Inconel 625 components requires extensive machining to achieve the CAD-specified geometry. In response, additive manufacturing (AM) technologies have emerged as alternative approaches to address these limitations. Binder jet 3D printing (BJ3DP) is a non-beam additive manufacturing technique that supports the rapid fabrication of complex parts with near-isotropic properties. However, industrial adoption remains limited by the absence of optimized printing and sintering parameters necessary to achieve high-performance components. To address this gap, the present study investigates the influence of printing parameters (e.g., layer thickness, binder saturation ratio) and sintering conditions (e.g., temperature, holding time) on the quality of BJ3D printed parts. The quality was evaluated in terms of green/brown density, dimensional accuracy, and surface roughness. The reported data will contribute to the development of semi-predictive models that bridge the gap between process parameters and mechanical properties. Such models will reduce the reliance on trial-and-error approaches and support the industrial adoption of BJ3DP in major industrial sectors such as aerospace, energy, and defence.

Keywords Binder jetting · IN625 · Layer thickness · Binder saturation · Surface roughness

Introduction

Inconel 625 (IN625) is a Nickel-based superalloy widely used in aerospace, defense, and energy industries due to its excellent mechanical performance, corrosion resistance, and stability under extreme temperature and pressure conditions. However, the alloy's high strength and work-hardening behavior render conventional subtractive manufacturing processes time-consuming and costly due to extensive tool wear. Consequently, additive manufacturing (AM) has emerged as an effective alternative for producing complex geometries directly from CAD models, particularly for such difficult-to-machine materials. Among metal AM technologies, binder jet 3D printing (BJ3DP) offers advantages such as high build rates and scalability compared with laser powder bed fusion. In BJ3DP, a liquid binder locally joins powder particles layer-by-layer to form a green part that subsequently undergoes curing, debinding, and sintering; while the absence of localized melting reduces residual stresses and distortion, final part quality remains strongly dependent on the selection of printing and post-processing parameters [1-6].

Although previous studies have explored various aspects of binder jet 3D printing of IN625, a systematic experimental mapping of process–property relationships—linking printing parameters to intermediate part quality (green and brown states), dimensional accuracy, and surface roughness—remains incomplete. The present study addresses this gap by experimentally examining the influence of key printing parameters such as layer thickness and binder saturation ratio and sintering conditions, including temperature and holding time—on green and brown density, dimensional accuracy, and surface roughness of binder-jetted IN625 parts. The resulting dataset supports the development of semi-predictive models that will reduce the reliance on trial-and-error optimization and promote industrial adoption of BJ3DP in major industrial sectors.

Mohamed A. Abbas · M Faisal Riyad · Sun Woong Kim · Nathan Fonseca · Shams Torabnia · Pu Han · Keng Hsu
School of Manufacturing Systems and Networks, Arizona State University, Mesa, AZ 85212, USA
e-mail: mohamed.abbas@asu.edu; faisal.riyad@asu.edu; sunwoon1@asu.edu; nfonsec1@asu.edu; storabnia@asu.edu; Pu.Han@asu.edu; Keng.H.Hsu@asu.edu

© The Author(s), under exclusive license to River Publishers 2026

Piyush Thakre et al. (eds.), *Mechanics of Additive and Advanced Manufacturing, Inverse Methods and Machine Learning, Volume 5, 2026*, Conference Proceedings of the Society for Experimental Mechanics Series, https://doi.org/10.13052/rp-9788743815983

Experimental procedures

Gas-atomized IN625 powder supplied by Carpenter Powder Products was used in this study, and its chemical composition, as specified in the material data sheet, is listed in Table 1. The powder morphology, surface texture, and particle size distribution (PSD) were characterized using a Phenom Pharos G2 scanning electron microscope and a Malvern Morphologi 4 particle size analyzer. The complete experimental procedure is summarized in the workflow diagram shown in Figure 1. In this study, the X direction corresponds to the powder spreading (recoating) direction, the Y direction corresponds to the printhead scanning direction, and the Z direction represents the build (layer stacking) direction. Cubic coupons ($15 \times 15 \times 15$ mm^3) were printed using an ExOne Innovent+ binder jet 3D printer with an aqueous polymer binder (BA005). The default printing parameters were set as follows: drying time of 10 s, recoat speed of 300 mm/s, roller traverse speed of 3 mm/s, and roller rotation speed of 600 rpm. To assess the influence of printing parameters, layer thickness and binder saturation ratio were systematically varied. The layer thicknesses were set to 75 µm, 100 µm, and 150 µm, while binder saturation levels were adjusted to 40%, 65%, and 95%. All other printing parameters were kept constant. Sixteen samples were fabricated for each parameter combination to ensure repeatability. To improve green strength, the as-printed parts were cured at 200 °C for 6 h in a Yamato DX402C drying oven, and excess powder was subsequently removed using soft brushing. The reclaimed powder was then dried overnight to remove residual moisture and reused for subsequent printing experiments.

Table 1 Chemical composition of Inconel 625 powder provided by Carpenter Powder Products (wt.%).

Element	Ni	Cr	Mo	Nb	Fe	Ti	Al	O	N	C
Wt.%	64.18	21.03	9.37	4.02	0.86	0.24	0.15	0.018	0.012	0.03

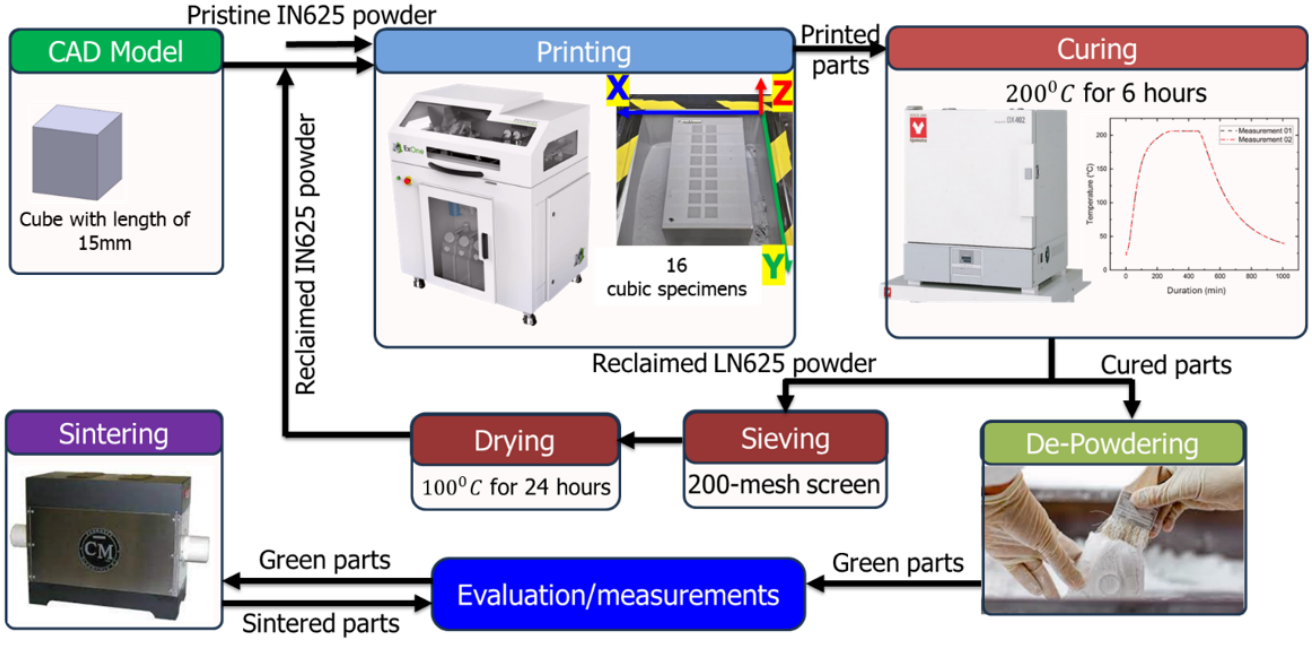

Fig. 1 Flow chart of the experimental procedure.

The influence of printing parameters on the quality and densification of green parts after curing was evaluated by measuring density, dimensional accuracy, and surface roughness. Green density was determined by measuring the mass using a high-precision balance (0.1 mg resolution) and the dimensions using a digital caliper (0.01 mm resolution). The theoretical density of IN625 was taken as 8.44 g/cm^3 at room temperature. Dimensional deviation was evaluated by comparing the green part dimensions with the original CAD model in the X, Y, and Z directions to assess the isotropy of shrinkage behavior, as defined by Equation (1).

$$Deviation_i\,(\%) = \frac{L_{i,\,measured} - L_{i,\,CAD}}{L_{i,\,CAD}} * 100 \tag{1}$$

where:$i = x, y, z$; $L_{i,\text{measured}}$ = measured dimension in the green state; and $L_{i,\text{CAD}}$ = original CAD dimension. The arithmetic mean surface roughness (Sa) of the green specimens was measured using a VHX-7000 digital microscope on three surfaces normal to the X, Y, and Z axes.

Results and discussion

The SEM and particle size distribution results are shown in Fig. 2. SEM images indicate that the IN625 powder has a predominantly spherical morphology, with some satellite particles attached to the surfaces of the larger particles, as illustrated in Fig. 2 (a). The particle size distribution shown in Fig. 2 (b) exhibits a single peak for both powders; however, the peak for the reclaimed powder is shifted slightly toward smaller particle sizes compared to the pristine powder. The images of the cured cubic specimens produced under different parameter combinations are shown in Fig. 3. As observed, samples printed

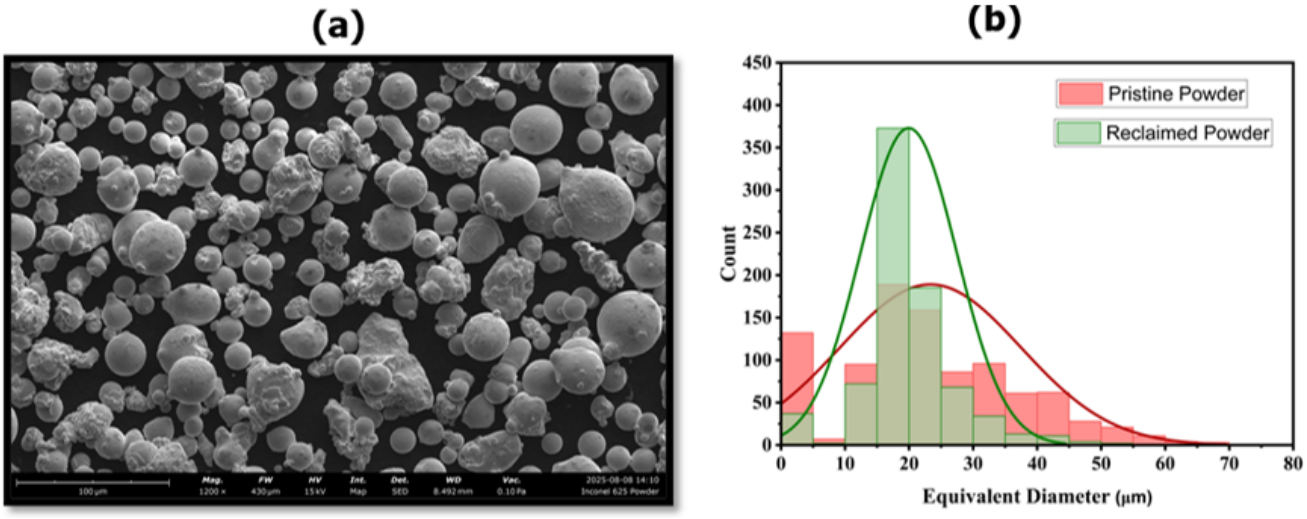

Fig. 2 (a) SEM morphology of IN625 powder; (b) comparison of particle size distributions for pristine and reclaimed powders.

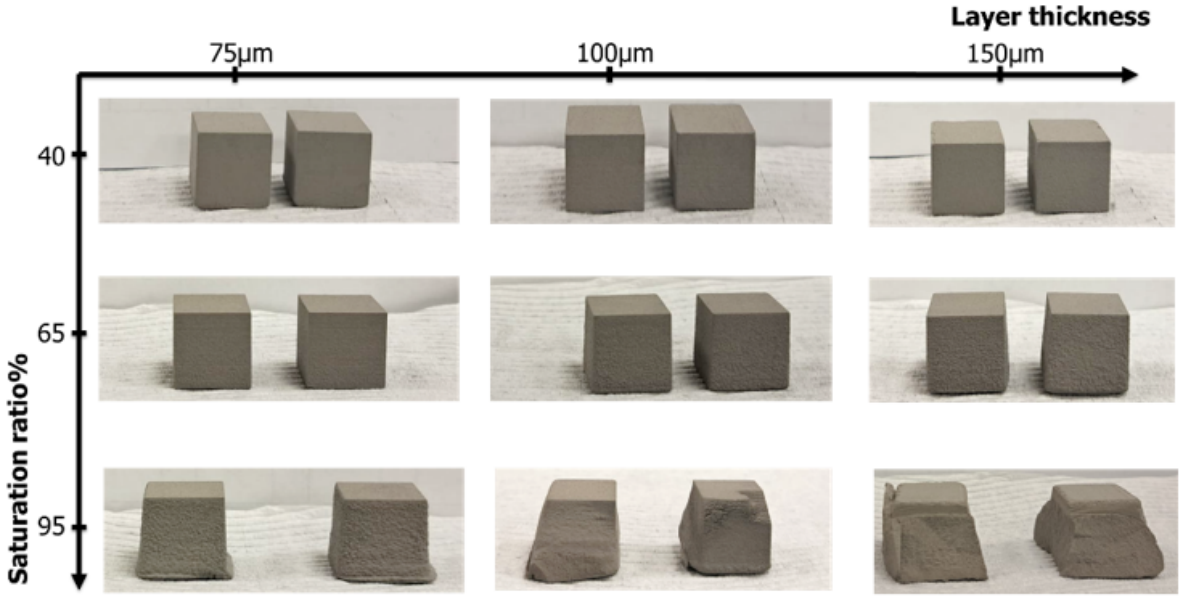

Fig. 3 Cured cubic specimens printed with varying layer thickness and binder saturation ratios.

with a binder saturation ratio of 95% exhibit a pronounced "elephant foot" effect, characterized by outward expansion at the base of the part. This distortion results from excess binder spreading beyond the intended boundaries, causing the lower layers to exceed the nominal CAD dimensions. The severity of this effect decreases progressively with lower binder saturation levels and reduced layer thickness.

The influence of layer thickness and binder saturation ratio on green density after curing is shown in Figure 4. Specimens printed with a layer thickness of 75 μm exhibited slightly higher relative density compared to those printed at 150 μm across all saturation levels. Thinner layers promote improved packing and more uniform binder distribution, resulting in reduced interlayer porosity. In the meantime, increasing the binder saturation ratio from 40% to 65% led to a slight increase in green density. However, this trend was not observed at 95% saturation, likely due to the significant dimensional distortion at this level, which made accurate measurements with the caliper more challenging. Dimensional deviation in the X, Y, and Z directions was calculated using Equation (1), and the results are also presented in Fig. 3. An increase in binder saturation led to greater dimensional deviation in the X and Y directions, primarily due to binder spreading that caused in-plane expansion. Similarly, increasing the layer thickness further amplified dimensional deviation, with the effect becoming more pronounced at higher saturation levels.

The arithmetic surface roughness (Sa), measured on planes normal to the X, Y, and Z axes, is presented in Figure 5. Specimens printed with a 95% binder saturation ratio exhibited dimensional deviations greater than 10% and were therefore excluded from the surface roughness analysis. Among the three measurement planes, surfaces normal to the Z axis generally showed lower roughness compared to those normal to the X and Y directions. Increasing the layer thickness did not

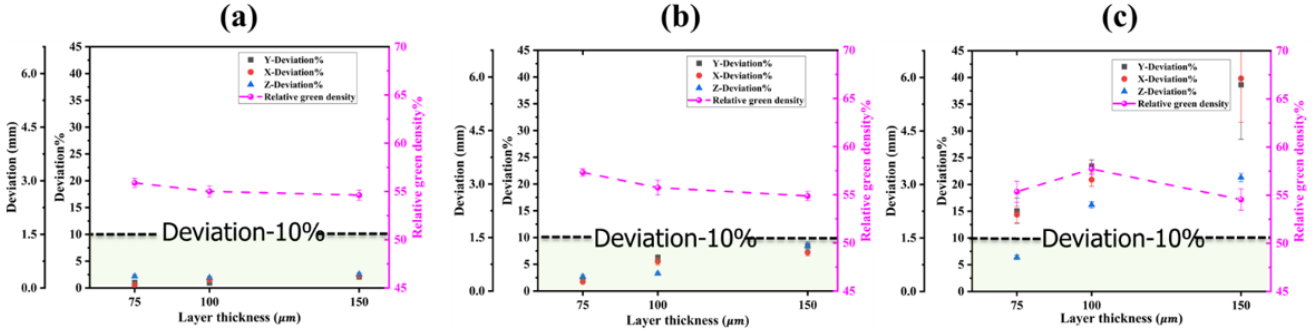

Fig. 4 Influence of layer thickness on green density and dimensional deviation at different binder saturation levels: (a) 40%, (b) 65%, and (c) 95%.

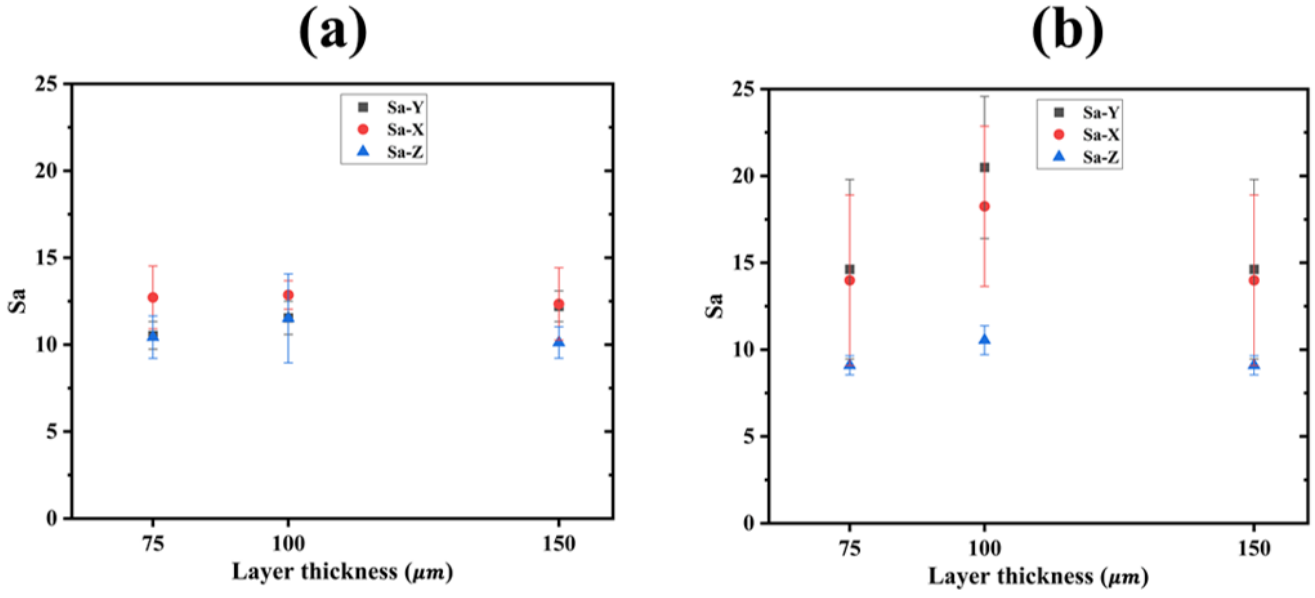

Fig. 5 Surface roughness (Sa) as a function of layer thickness at binder saturation levels of (a) 40% and (b) 65%.

significantly affect surface roughness. In contrast, higher binder saturation ratios resulted in a noticeable increase in surface roughness, particularly in the X and Y directions.

Conclusion and Future Work

This study examined the effects of layer thickness and binder saturation ratio on the quality of binder jet printed Inconel 625 green parts. Green density, dimensional deviation, and surface roughness were evaluated to establish process–property relationships. Thinner layers (75 μm) improved green density due to enhanced packing and more uniform binder distribution. Increasing binder saturation from 40% to 65% slightly increased density; however, excessive saturation (95%) caused significant dimensional distortion, including a pronounced "elephant foot" effect due to binder spreading. Dimensional deviation increased with binder saturation, particularly in the X and Y directions, while surface roughness was also more sensitive to saturation than to layer thickness. Surfaces normal to the Z direction generally exhibited lower roughness values. Future work will focus on optimizing sintering parameters, characterizing microstructure and phase evolution, evaluating mechanical properties, and developing predictive models to link processing parameters to final part performance.

References

1. Karmuhilan, M., and Somasundaram Kumanan. "A review on additive manufacturing processes of Inconel 625." Journal of Materials Engineering and Performance 31, no. 4 (2022): 2583-2592.
2. Dudzinski, D., Devillez, A., Moufki, A., Larrouquère, D., Zerrouki, V. and Vigneau, J., "A review of developments towards dry and high speed machining of Inconel 718 alloy." International journal of machine tools and manufacture 44, no. 4 (2004): 439-456.
3. Li, Ming, Wenchao Du, Alaa Elwany, Zhijian Pei, and Chao Ma. "Metal binder jetting additive manufacturing: a literature review." *Journal of Manufacturing Science and Engineering* 142, no. 9 (2020): 090801.
4. Mostafaei, Amir, Erica L. Stevens, Eamonn T. Hughes, Shannon D. Biery, Colleen Hilla, and Markus Chmielus. "Powder bed binder jet printed alloy 625: Densification, microstructure and mechanical properties." *Materials & Design* 108 (2016): 126-135.
5. Gonzalez, J. A., J. Mireles, S. W. Stafford, M. A. Perez, C. A. Terrazas, and R. B. Wicker. "Characterization of Inconel 625 fabricated using powder-bed-based additive manufacturing technologies." *Journal of Materials Processing Technology* 264 (2019): 200-210.
6. Zheng, Chuyuan, Amir Mostafaei, Pierangeli Rodriguez de Vecchis, Ian Nettleship, and Markus Chmielus. "Microstructure evolution for isothermal sintering of binder jet 3D printed alloy 625 above and below the solidus temperature." *Additive Manufacturing* 47 (2021): 102276.